



Published in final edited form as:

*J Neurooncol.* 2011 November ; 105(2): 365–373. doi:10.1007/s11060-011-0601-x.

## Proton magnetic resonance spectroscopy predicts survival in children with diffuse intrinsic pontine glioma

Emilie A. Steffen-Smith<sup>1</sup>, Joanna H. Shih<sup>2</sup>, Sean J. Hipp<sup>1,3,4</sup>, Robyn Bent<sup>1</sup>, and Katherine E. Warren<sup>1</sup>

<sup>1</sup>Pediatric Oncology Branch, Center for Cancer Research, National Cancer Institute, National Institutes of Health, 9000 Rockville Pike, Bethesda, MD

<sup>2</sup>Biometric Research Branch, Division of Cancer Treatment and Diagnosis, National Cancer Institute, National Institutes of Health, 9000 Rockville Pike, Bethesda, MD

<sup>3</sup>Walter Reed Army Medical Center, Department of Pediatrics, Washington, DC

<sup>4</sup>Uniformed Services University of the Health Sciences, Department of Pediatrics, Bethesda, MD

### Abstract

Patients with diffuse intrinsic pontine glioma (DIPG) face a grim prognosis with limited treatment options. Many patients will enroll on investigational trials though the role of chemotherapy or immunotherapy is unclear. Radiographic changes on conventional MRI are used to evaluate tumor response and progression, but are not predictive of outcome in these patients. More sensitive measures of tumor biology are needed to improve patient management. We evaluated changes in magnetic resonance spectroscopy (MRS) biomarkers in patients with DIPG. Thirty-eight patients were enrolled prospectively on an IRB-approved protocol, which included standard MRI, single voxel spectroscopy (SVS) and multi-slice multi-voxel spectroscopy (MRSI). Scans were performed at multiple time points during each patient's clinical course, with a total of 142 scans. The prognostic values of Choline:N-acetylaspartate (Cho:NAA), Cho:Creatine (Cho:Cr) and the presence of lactate and lipids (+Lac/Lip) were evaluated. Cho:NAA and variance in Cho:NAA values among different voxels within a tumor were each predictive of shorter survival. This prospective study shows that MRS can be used to identify high-risk patients and monitor changes in tumor metabolism, which may reflect changes in tumor behavior.

### Keywords

pediatric; brain; brainstem tumor; MRI; MR spectroscopy; prognosis

### Introduction

Diffuse intrinsic pontine glioma (DIPG) remains one of the most challenging solid tumors to treat in children. The incidence of these tumors is rare, with an estimated 300 children diagnosed in the United States each year [1]. Age of onset is most commonly 5–9 years, though cases may occur from infancy to adulthood [2–5]. Median survival for children with DIPG is less than 1 year and has remained unchanged in the past three decades [6]. The

**Corresponding Author:** Katherine E. Warren, M.D., Pediatric Oncology Branch, National Cancer Institute, Building 10/Room 1-5750, 9000 Rockville Pike, Bethesda, MD 20892, Phone: 301-435-4683, FAX: 301-480-2308, warrenk@mail.nih.gov.

This work was presented in part at the ASNR 47<sup>th</sup> Annual Meeting, Vancouver 2009.

The views expressed in this article are those of the authors and do not reflect the official policy of the National Institutes of Health, Department of Army, Department of Defense, or U.S. Government.

infiltrative nature and location of DIPG precludes surgical intervention. Patients are diagnosed and followed using conventional magnetic resonance imaging (MRI), though imaging characteristics including tumor size, tumor extent, necrosis and encapsulation of the basilar artery are not prognostic and have limited utility in evaluating response to treatment [7–9]. Radiation therapy is the standard treatment, providing transient palliation of neurological symptoms in 75 – 85% of patients [6, 10, 11]. Chemotherapeutic agents have made no improvement in patient outcome to date, and many children enroll on investigational trials [6, 12–18]. To improve treatment of patients with DIPG, a better understanding of tumor biology is needed. Biopsy of the brainstem remains controversial, and is typically only performed to confirm diagnosis in patients with an atypical presentation [16, 19, 20]. Tissue analysis is therefore limited largely to specimens collected post-mortem from a small number of patients [21–23]. Histological grading of biopsy tissue varies; however, the majority of autopsy cases are high-grade [24]. The pathophysiology of DIPG is poorly understood, and a comprehensive understanding of tumor behavior over the disease course is lacking.

Metabolic imaging techniques such as positron emission tomography (PET) and magnetic resonance spectroscopy (MRS) provide an *in vivo* analysis of the functional behavior of tumors and surrounding tissues. MRS is non-invasive and allows repeated measurements of multiple metabolites. The concentrations of tissue metabolites reflect physiologic changes in the tumor environment. In pediatric CNS tumors, changes in MRS metabolic markers are predictive of tumor grade [25, 26], tumor progression [27] and overall patient survival [28, 29] in a limited number of studies. Retrospective analyses of MRS in a small number of patients with DIPG have identified metabolic changes prior to disease progression [30–32]. The purpose of our study was to monitor changes in tumor metabolism in patients with DIPG using two MRS techniques—single voxel and multi-slice multi-voxel spectroscopy—and to evaluate the relationship between MRS biomarkers and overall survival.

## Materials and Methods

### Patients

Patients (< 21 years) were referred to our institution for evaluation of a newly diagnosed, refractory or progressive DIPG. Each patient's diagnosis was confirmed using stringent criteria specific to DIPG: 1) clinical symptoms at diagnosis, including cranial nerve deficits, long tract signs or ataxia and 2) radiographic findings of a lesion centered in the pons with diffuse signal hyperintensity involving > 50% of the pons on a T2-weighted sequence. Patients with primarily exophytic tumors were excluded. Prior or current treatment, including radiation therapy, was not an exclusion criterion. Patients' legal guardians were consented for a protocol approved by the National Cancer Institute's Institutional Review Board.

### Imaging

Patients were monitored with standard and advanced MRI techniques using a Signa HDx 1.5T scanner (GE Medical Systems, Milwaukee WI) with a standard quadrature head coil. MRI studies were performed according to this imaging protocol and as clinically indicated. MRI sequences included pre- and post-contrast T1-weighted spin echo (TR/TE = 450/13 ms, FOV = 22×22 cm, matrix = 256×192, 50 slices, slice thickness=3 mm, no gap), T2-weighted fast spin echo (TR/TE = 3400/95 ms, FOV = 22 × 22 cm, matrix = 256 × 192, 53 slices, slice thickness = 3 mm, no gap) and fluid attenuated inversion recovery (FLAIR; TR/TE/TI = 10,000/140/2200 ms, FOV = 22 × 22 cm, matrix = 256×192, 53 slices, slice thickness = 3 mm, no gap). Contrast enhanced images were acquired after MRS.

Single voxel spectroscopy (SVS) was obtained using a point-resolved spectroscopic sequence (PROBE-P, GE Medical Systems) with automated shimming and water suppression (TR/TE = 1500/144 or 270 ms, FOV = 22×22 cm, averages = 128, slice thickness = 15 or 20 mm). Voxels were prescribed graphically on a pre-contrast axial T2-weighted image and centered on the lesion, posterior to the basilar artery while avoiding areas of CSF, bone, and subcutaneous fat. Voxel size varied according to the size of the tumor, with a minimum size of 3 cm<sup>3</sup>. Acquisition time was approximately 3.5 minutes.

Multi-slice magnetic resonance spectroscopic imaging (MRSI) was used to collect data from multiple voxels simultaneously. MRSI slices were positioned at the same locations as a T1-weighted axial oblique localizer sequence (TR/TE = 50/3.5 ms, FOV = 24 × 24 cm, matrix = 256 × 160, slice thickness = 15 mm, slice space = 3.5 mm). Slices were aligned such that the center of the one slice included the maximum tumor diameter within the pons. Parallel slices were obtained to evaluate parts of the tumor extending above or below the pons. MRSI acquisition used a slice-selective spin echo sequence (TR/TE = 2300/280 ms, FOV = 24 × 24 cm, matrix = 32 × 32, 4 slices, slice thickness = 15 mm, slice spacing = 3 mm) with a chemical shift selective (CHESS) water suppression pulse and octagonal outer volume saturation (OVS) to suppress lipid signals from the scalp and skull [33]. OVS bands were placed closer together in the inferior MRSI slices to reduce lipid contamination in the posterior fossa [34]. A 32 × 32 array of spectra from voxels, each with a nominal volume of 0.84 cm<sup>3</sup> (7.5 mm × 7.5 mm × 15 mm) was obtained for each of the four MRSI slices [33]. Acquisition was approximately 25 minutes.

### Data Processing and Analysis

SVS data were reconstructed using the automated PROBE/SVQ processing routine (GE Medical Systems) with frequency offsets for water-suppressed data and Marquardt curve fitting to determine peak amplitudes for major metabolites within the spectrum including N-acetyl-aspartate (NAA, 2.01 ppm), Choline (Cho, 3.20 ppm) and Creatine (Cr, 3.03 ppm). Peak amplitudes were used to calculate Cho:NAA and Cho:Cr ratios. For each SVS study, we also noted the presence or absence of lactate and lipids (Lac/Lip), defined by prominent peaks (signal:noise > 3:1) between 1.3 and 1.4 ppm.

Raw MRSI data were transferred to a Linux workstation for processing using a customized software package developed in IDL (ITT Visual Information Solutions, Boulder CO) [35]. Software provided automated selection of major metabolite peaks within each spectrum and generated signal intensity maps for NAA, Cho and Cr. Pre-contrast FLAIR images were imported and registered to MRSI slices using the orientation and location information from the image headers. Regions of interest (ROIs) were manually drawn on FLAIR images corresponding to the MRSI slice with the maximum tumor diameter in the pons. ROIs included all voxels within the FLAIR signal abnormality. Selected ROIs were simultaneously applied to metabolite signal intensity maps. Voxels outside the ROI were masked and excluded from further evaluation. ROI voxels with water or lipid contamination were nulled and excluded. All remaining ROI spectra were evaluated using automated quality control criteria as previously described [35]. Relative metabolite concentrations were reported as the integral of the area under the signal intensity peak for NAA, Cho, and Cr. Results for accepted ROI voxels were expressed as Cho:NAA and Cho:Cr ratios. A “worst voxel” analysis was applied to determine maximum Cho:NAA and maximum Cho:Cr for each study as previously described [28]. We evaluated tumor heterogeneity using the variance in Cho:NAA and Cho:Cr values within each MRSI region of interest.

## Statistical Analysis

Because we wanted to evaluate the prognostic significance of MRS at any time point in the disease course and MRS was not obtained at diagnosis for the majority of our patients due to the typical timing of patient referrals to our institution, the relationship between MRS measures and patient outcome was calculated as the length of time from the date of the MRS study to the date of death or last follow-up. Survival distributions using the median of each MRS measure ( $>$  or  $\leq$  median) were estimated using the Kaplan-Meier method and compared using a log-rank test. We used univariate Cox proportional hazards models to estimate the predictive effect of each SVS and MRSI measure on patient survival [36]. Variables used in the analysis included Cho:NAA, Cho:Cr and presence or absence of Lac/Lip for SVS, and the maximum and variance of Cho:NAA and Cho:Cr for MRSI. Two types of analyses were performed using these models 1) risk of death associated with each variable at the first imaging time point and 2) risk of death associated with changes in each variable from one time point to the next using follow-up data. For the second analysis, time-dependent covariates were incorporated in the Cox proportional hazards model to evaluate whether a change in a given MRS variable at follow-up increased a patient's risk of death [36]. Risk was expressed as a hazard ratio (HR) and represented the risk of mortality per one unit change in for each MRS variable.  $HR > 1$  corresponded to increased risk of death (i.e., shorter survival). Overall survival (OS) was also reported and defined as the length of time from the date of diagnosis to the date of death or last follow-up. OS for the patient cohort was calculated using the Kaplan-Meier method. P-values of  $< 0.05$  were considered statistically significant for all analyses. Data were analyzed using the statistical computing package, R (<http://www.r-project.org/>).

## Results

### Patients

Thirty-eight patients were included in this study. Clinical characteristics are summarized in Table 1. Thirty-six patients received radiation therapy prior to referral to our institution for study enrollment. Two patients were radiation-naïve because their families declined radiation therapy. The majority of patients ( $n = 36$ ) received therapy over the course of this study through concurrent enrollment in a variety of investigational trials of chemotherapeutic or biologic agents. At the time of last follow-up, 27 patients had died of disease and 9 patients remained on study. Median overall survival for the entire cohort was 14.8 months (Figure 1). Six patients (median age = 6.8 yr, range = 2.6 – 14.1 yr), had an overall survival (OS)  $> 24$  months. None of these patients underwent biopsy. These long-term survivors did not differ in presentation, age or treatment from patients with a typical disease course (OS  $< 24$  months), with the exception of one patient whose initial MRI scan and clinical presentation was atypical, and the family chose to delay radiation until the child's clinical status worsened. In that case, radiation therapy began 1559 days (over 51 months) after initial suspected diagnosis as the clinical and radiographic characteristics were more typical of DIPG.

### Imaging Studies

One hundred forty two scans with MRS were obtained over the course of this study. The first imaging studies were performed a median of 4.3 months after initial diagnosis (range = 2.0 – 58.6 months). Scans were performed following radiation therapy (RT) for patients who received it (median = 1.8 months post RT). Follow-up scans were obtained in 74% of patients ( $n = 28$ ), with a median of 4 scans per patient. Median duration of follow-up was 7.1 months (range = 1.6 – 61.6 months), with a median interval of 8 weeks between scans (range = 1 – 57 weeks).

## MRS analysis

SVS studies were obtained in all 38 patients. SVS volumes ranged from 3.4 – 20.7 cm<sup>3</sup> (median= 9.0 cm<sup>3</sup>). Lac/Lip was identified in 45% (n=17) of the first SVS scans, and 39% (n=56) of all SVS spectra. SVS Cho:NAA and Cho:Cr ranged from 0.6 – 5.9 (median = 2.1) and 1.0 – 5.2 (median = 2.0), respectively.

MRSI was obtained in 36 patients (95%). ROIs for MRSI studies included 4 to 28 voxels (median = 12 voxels), with 10% to 100% voxel acceptance (median = 80%). Maximum Cho:NAA and maximum Cho:Cr from MRSI ranged from 0.7 – 7.8 (median = 2.1) and 1.3 – 4.9 (median = 2.5), respectively. We evaluated the range in MRSI Cho:NAA and Cho:Cr values for each ROI. We observed less variance in Cho:Cr values (median variance = 0.08) compared to Cho:NAA values (median variance = 0.20) within the same ROIs. The maximum Cho:NAA and variance of values were highly correlated ( $r=0.97$ ). As the maximum Cho:NAA increased, the variance of Cho:NAA values throughout the ROI also increased.

## Survival Analyses

Results for the survival analyses using the univariate Cox proportional hazards model are presented in Table 2. The analysis of the MRS measures from the first imaging study found that SVS Cho:NAA was the only variable predictive of patient survival ( $p = 0.03$ ). Patients with higher SVS Cho:NAA values at their first scan were at greater risk of mortality compared to patients with lower SVS Cho:NAA values. The relationship between presence of SVS Lac/Lip and survival reached borderline significance ( $p = 0.08$ ), but SVS Cho:Cr was not significant ( $p = 0.20$ ). None of the measures obtained by MRSI, had a significant prognostic effect on patient survival ( $p > 0.05$ ). Kaplan-Meier estimates using the median of MRS measurements from a single time point (i.e., the first MRS scan) did not show a significant difference in patient survival ( $p > 0.05$ ).

The time-dependent covariate analysis of follow-up SVS studies yielded similar results to the analysis of SVS variables from first scan (Table 2). Changes in Cho:Cr values and the presence of Lac/Lip were not predictive of patient outcome ( $p = 0.29$  and  $p = 0.18$ , respectively). However, an increase in SVS Cho:NAA from one time point to the next, regardless of the Cho:NAA value at the first time point, had a significant inverse association with patient survival ( $p = 0.009$ ). Patients whose SVS Cho:NAA values were increased at follow-up were at greater risk of death compared to patients with stable or decreased SVS Cho:NAA. Prognosis worsened relative to the amount of increase in SVS Cho:NAA (i.e., the larger increase in Cho:NAA, the poorer the prognosis), and decreases in SVS Cho:NAA at follow-up reduced a patient's risk of death (Table 3). Figure 2 illustrates the changes in SVS Cho:NAA values for 4 patients over the course of the study.

We evaluated the prognostic effect of changes at follow-up for the maximum and variance of Cho:NAA and Cho:Cr values as determined by MRSI. Maximum and variance in Cho:Cr were not predictive of patient survival ( $p = 0.53$  and  $p = 0.36$ , respectively). The risk of death associated with an increase in maximum Cho:NAA from one time point to the next reached borderline significance ( $p = 0.06$ ). Increases in the variance of MRSI Cho:NAA values were associated with decreased patient survival ( $p = 0.03$ ). The amount of increase was directly related to the risk of death (Table 3). Patients whose tumors became more metabolically heterogeneous over time (i.e., greater variance in Cho:NAA values) had a markedly increased risk of death compared to patients with more stable, uniform Cho:NAA values. Figure 3 illustrates the changes in Cho:NAA variance for one patient.

Using the Cox proportional hazards models, we found that SVS Cho:NAA values obtained at any time point had a prognostic effect on patient survival. To further characterize the



predictive value of SVS Cho:NAA, we evaluated the median SVS Cho:NAA from the follow-up analysis (SVS Cho:NAA= 2.1) as a potential threshold for identifying high-risk patients. Patients with SVS Cho:NAA  $\geq$  2.1 had a marked increased risk of death compared to those with SVS Cho:NAA  $<$  2.1 (HR = 2.48,  $p = 0.04$ ). The majority of patients ( $n = 29$ ) had at least one scan with SVS Cho:NAA  $\geq$  2.1, and median OS was 9 months (95% CI = 7.8 – 12.2). A subgroup of these patients ( $n=15$ ) had SVS Cho:NAA  $\geq$  2.1 for all time points (median OS = 8.7 months, 95% CI = 4.4 – 12.5+). Only nine patients had SVS Cho:NAA  $<$  2.1 for all time points. OS was increased for these patients, with a median OS of 12.3 months (95% CI = 7.7 – 51.0+).

## Discussion

This study shows that metabolite ratios obtained from proton spectroscopic methods in children with DIPG are prognostic. These include Cho:NAA obtained from single voxel spectroscopy and performed at any time point in the disease course, as well as changes in Cho:NAA over time. In addition, increasing variation of Cho:NAA within tumor voxels as determined by multi-voxel spectroscopy was also indicative of a poorer outcome. The correlation of changes in Cho:NAA over time and outcome suggests that the techniques can be used to determine tumor progression or tumor response to treatment and may therefore be a potentially useful noninvasive biomarker.

The evaluation of children with DIPG over their disease course is complicated due to restrictions on obtaining tumor tissue samples. MRS techniques provide unique biochemical information from tissue *in vivo*, and are frequently used to interrogate the metabolic behavior of adult and pediatric primary brain tumors [25–27, 37, 38]. Because of the lack of standardization, the role of proton spectroscopy in patient management has been unclear. It has been used in adult patients with supratentorial tumors to assist treatment planning, including surgical intervention, selection of biopsy targets, and evaluation of response to therapy [39, 40]. However, given the added limitations of performing spectroscopy in the posterior fossa and the predominantly poor prognosis of these patients, the clinical utility of MRS for patients with DIPG is still undefined. Having objective noninvasive measures for prognosis, progression and response represent key advances in the management of these patients.

It is difficult to define tumor progression in children with DIPG using standard WHO criteria with two-dimensional tumor measurements. Criteria for tumor progression are generally defined by both clinical symptoms and imaging characteristics. Radiographic tumor measurements are highly variable [41], and treatment-related changes such as radiation necrosis and progressive disease are not easily distinguished using standard MRI [7, 8, 42–44]. To avoid the subjectivity associated with identifying tumor progression by tumor measurement, we used overall survival rather than time to progression for our analysis. Proton MRS, and in particular, Cho:NAA, can be indicative of changes in cellularity [45, 46]. Cho is a component of cell membranes, while NAA is found primarily in normal functioning neurons. Increased Cho:NAA can be associated with increased number of cells, increased cell turnover, damaged neurons or a combination. These changes may be present and identified by MRS prior to seeing anatomic changes on MRI [46, 47].

Limitations of prior MRS studies have been the identification of defined Cho:NAA threshold values associated with overall survival and the identification of meaningful changes in Cho:NAA. Studies of children with brain tumors evaluated heterogeneous groups of patients, and included a small number of brainstem gliomas [28, 29]. One previous study of patients with DIPG explored the relationship between baseline MRS data and survival in patients with DIPG using a short echo time (TE = 35ms) SVS technique [31]. Results were

not significant, but the study was limited by a small number of patients ( $n = 12$ ). In our study, we identified a threshold value, Cho:NAA = 2.1, that allows stratification of patients by risk. Patients who remained below this threshold had significantly longer survival compared to patients who had at least one scan with Cho:NAA  $\geq 2.1$ . We were also able to show that *any* increase in Cho:NAA over time was significant, and the degree of change directly impacted the risk.

In adult gliomas, the association between increased Cho:NAA and increased histological grade has been established, and regional differences in Cho:NAA reflect the heterogeneous growth patterns found within the same lesion [37, 38, 48–51]. Higher grade tumors may have more intratumoral heterogeneity in Cho:NAA values, with areas of the highest Cho:NAA indicating more aggressive regions of the tumor, while regions of lower Cho:NAA are found in less aggressive tumor or even normal tissue within the lesion [37, 51]. Likewise, variance of Cho:NAA values, which indicates metabolic heterogeneity, was associated with an increased risk of death in our study.

These study results should be interpreted with recognition of some limitations. Our study included 6 patients (16%) whose overall survival was  $> 24$  mo. This represents a larger proportion of long-term survivors when compared some studies [6], but is comparable to other cohorts reported in the literature [31, 52]. The majority of patients were referred to our institution following radiation therapy for evaluation after disease progression. As such, MRS was not obtained at diagnosis, thereby limiting the evaluation of the effects of individual treatment regimens. Given the number of different treatment regimens, stratification according to treatment regimen or time since treatment was not possible without compromising the statistical power of the study.

Technical restrictions should also be considered. Acquisition of MRS in the brainstem is more difficult compared to supratentorial MRS studies. Proximity of air, bone, and subcutaneous fat may cause magnetic field inhomogeneity, resulting in baseline distortion, poor spectral resolution and lipid contamination [34, 53–56]. SVS and MRSI was successfully obtained in the majority of our patients; however, for some MRSI cases, voxel acceptance within ROIs was  $< 100\%$  or relative NAA concentrations were too low to distinguish from baseline noise. As such, the maximum Cho:NAA obtained by MRSI was not necessarily representative of the highest grade or most aggressive area of the tumor. Other technical confounds included lack of registration for follow-up scans and voxel selection. MRSI and SVS regions of interest were analyzed by a single spectroscopist and matched in location as closely as possible to previous time points, using similar slice locations for each patient, but co-registration of spectroscopic data on follow-up scans was not possible. Regions of interest changed in size with tumors to ensure maximum coverage of the lesion based on the signal abnormality on MRI. For MRSI data, ROIs were selected to include areas of signal abnormality on the structural FLAIR images. Areas of necrosis, edema and blood products may have been included as these pathological conditions are difficult to distinguish from tumor on standard MRI.

## Conclusion

MRS is a clinically relevant technique for evaluating patients with DIPG, identifying high-risk patients and predicting survival. Because changes in tumor metabolism, as identified by Cho:NAA and increasing metabolic heterogeneity, were prognostic, this technique can potentially be used as a surrogate marker of response or progression. While all patients with DIPG face a poor outcome, these results show that some patients are at higher risk of mortality than others. Assessment at diagnosis and continued follow-up of Cho:NAA during

therapy is recommended to evaluate patient prognosis, predict changes in tumor behavior, and assess treatment response.

## Acknowledgments

The authors thank Dr. Alan Barnett and Dr. Jan Willem van der Veen for their contributions towards the MRSI acquisition and data analysis. Research was supported in part by the Intramural Research Program of the National Institutes of Health, National Cancer Institute, Center for Cancer Research.

## References

1. Central Brain Tumor Registry of the United States (CBTRUS). CBTRUS statistical report: primary and central nervous system tumors diagnosed in the United States in 2004–2006. Hindsdale, IL: 2010. p. 10-25.
2. Ueoka DI, Nogueira J, Campos JC, Maranhao Filho P, Ferman S, Lima MA. Brainstem gliomas--retrospective analysis of 86 patients. *J Neurol Sci.* 2009; 281:20–23. [PubMed: 19345380]
3. Wolff JE, Classen CF, Wagner S, Kortmann RD, Palla SL, Pietsch T, Kuhl J, Gnekow A, Kramm CM. Subpopulations of malignant gliomas in pediatric patients: analysis of the HIT-GBM database. *J Neurooncol.* 2008; 87:155–164. [PubMed: 18209954]
4. Shah NC, Ray A, Bartels U, Rutka J, Bouffet E, Drake J, Hawkins CE, Huang A. Diffuse intrinsic brainstem tumors in neonates. Report of two cases. *J Neurosurg Pediatr.* 2008; 1:382–385. [PubMed: 18447673]
5. Maria BL, Rehder K, Eskin TA, Hamed LM, Fennell EB, Quisling RG, Mickle JP, Marcus RB Jr, Drane WE, Mendenhall NP, et al. Brainstem glioma: I. Pathology, clinical features, and therapy. *J Child Neurol.* 1993; 8:112–128. [PubMed: 8505473]
6. Hargrave D, Bartels U, Bouffet E. Diffuse brainstem glioma in children: critical review of clinical trials. *Lancet Oncol.* 2006; 7:241–248. [PubMed: 16510333]
7. Hargrave D, Chuang N, Bouffet E. Conventional MRI cannot predict survival in childhood diffuse intrinsic pontine glioma. *J Neurooncol.* 2008; 86:313–319. [PubMed: 17909941]
8. Liu AK, Brandon J, Foreman NK, Fenton LZ. Conventional MRI at presentation does not predict clinical response to radiation therapy in children with diffuse pontine glioma. *Pediatr Radiol.* 2009; 39:1317–1320. [PubMed: 19657635]
9. Kornreich L, Schwarz M, Karmazyn B, Cohen IJ, Shuper A, Michovitz S, Yaniv I, Fenig E, Horev G. Role of MRI in the management of children with diffuse pontine tumors: a study of 15 patients and review of the literature. *Pediatr Radiol.* 2005; 35:872–879. [PubMed: 15918050]
10. Freeman CR, Farmer JP. Pediatric brain stem gliomas: a review. *Int J Radiat Oncol Biol Phys.* 1998; 40:265–271. [PubMed: 9457808]
11. Broniscer A, Gajjar A. Supratentorial high-grade astrocytoma and diffuse brainstem glioma: two challenges for the pediatric oncologist. *Oncologist.* 2004; 9:197–206. [PubMed: 15047924]
12. Kim CY, Kim SK, Phi JH, Lee MM, Kim IA, Kim IH, Wang KC, Jung HL, Lee MJ, Cho BK. A prospective study of temozolomide plus thalidomide during and after radiation therapy for pediatric diffuse pontine gliomas: preliminary results of the Korean Society for Pediatric Neuro-Oncology study. *J Neurooncol.* 2010
13. Jalali R, Raut N, Arora B, Gupta T, Dutta D, Munshi A, Sarin R, Kurkure P. Prospective evaluation of radiotherapy with concurrent and adjuvant temozolomide in children with newly diagnosed diffuse intrinsic pontine glioma. *Int J Radiat Oncol Biol Phys.* 2010; 77:113–118. [PubMed: 19647954]
14. Korones DN, Fisher PG, Kretschmar C, Zhou T, Chen Z, Kepner J, Freeman C. Treatment of children with diffuse intrinsic brain stem glioma with radiotherapy, vincristine and oral VP-16: a Children's Oncology Group phase II study. *Pediatr Blood Cancer.* 2008; 50:227–230. [PubMed: 17278121]
15. Massimino M, Spreafico F, Biassoni V, Simonetti F, Riva D, Trecate G, Giombini S, Poggi G, Pecori E, Pignoli E, Casanova M, Ferrari A, Meazza C, Luksch R, Terenziani M, Cefalo G, Podda M, Polastri D, Clerici CA, Fossati-Bellani F, Gandola L. Diffuse pontine gliomas in children:



- changing strategies, changing results? A mono-institutional 20-year experience. *J Neurooncol.* 2008; 87:355–361. [PubMed: 18217208]
16. Frazier JL, Lee J, Thomale UW, Noggle JC, Cohen KJ, Jallo GI. Treatment of diffuse intrinsic brainstem gliomas: failed approaches and future strategies. *J Neurosurg Pediatr.* 2009; 3:259–269. [PubMed: 19338403]
  17. Michalski A, Bouffet E, Taylor RE, Hargrave D, Walker D, Picton S, Robinson K, Pizer B, Bujkiewicz S. The addition of high-dose tamoxifen to standard radiotherapy does not improve the survival of patients with diffuse intrinsic pontine glioma. *J Neurooncol.* 2010
  18. Broniscer A, Baker JN, Tagen M, Onar-Thomas A, Gilbertson RJ, Davidoff AM, Panandiker AP, Leung W, Chin TK, Stewart CF, Kocak M, Rowland C, Merchant TE, Kaste SC, Gajjar A. Phase I study of vandetanib during and after radiotherapy in children with diffuse intrinsic pontine glioma. *J Clin Oncol.* 2010; 28:4762–4768. [PubMed: 20921456]
  19. Pincus DW, Richter EO, Yachnis AT, Bennett J, Bhatti MT, Smith A. Brainstem stereotactic biopsy sampling in children. *J Neurosurg.* 2006; 104:108–114. [PubMed: 16506498]
  20. Perez-Gomez JL, Rodriguez-Alvarez CA, Marhx-Bracho A, Rueda-Franco F. Stereotactic biopsy for brainstem tumors in pediatric patients. *Childs Nerv Syst.* 2010; 26:29–34. [PubMed: 19784659]
  21. Zarghooni M, Bartels U, Lee E, Buczkowicz P, Morrison A, Huang A, Bouffet E, Hawkins C. Whole-genome profiling of pediatric diffuse intrinsic pontine gliomas highlights platelet-derived growth factor receptor alpha and poly (ADP-ribose) polymerase as potential therapeutic targets. *J Clin Oncol.* 2010; 28:1337–1344. [PubMed: 20142589]
  22. Gilbertson RJ, Hill DA, Hernan R, Kocak M, Geyer R, Olson J, Gajjar A, Rush L, Hamilton RL, Finkelstein SD, Pollack IF. ERBB1 is amplified and overexpressed in high-grade diffusely infiltrative pediatric brain stem glioma. *Clin Cancer Res.* 2003; 9:3620–3624. [PubMed: 14506149]
  23. Paugh BS, Qu C, Jones C, Liu Z, Adamowicz-Brice M, Zhang J, Bax DA, Coyle B, Barrow J, Hargrave D, Lowe J, Gajjar A, Zhao W, Broniscer A, Ellison DW, Grundy RG, Baker SJ. Integrated molecular genetic profiling of pediatric high-grade gliomas reveals key differences with the adult disease. *J Clin Oncol.* 2010; 28:3061–3068. [PubMed: 20479398]
  24. Sanai, N.; Prados, M. Brainstem Gliomas. In: Gupta, N.; Banerjee, A.; Haas-Kogan, DA., editors. *Pediatric CNS Tumors.* 1st edn.. Berlin: Springer; 2010. p. 49-65.
  25. Peet AC, Lateef S, MacPherson L, Natarajan K, Sgouros S, Grundy RG. Short echo time 1 H magnetic resonance spectroscopy of childhood brain tumours. *Childs Nerv Syst.* 2007; 23:163–169. [PubMed: 17106750]
  26. Astrakas LG, Zurakowski D, Tzika AA, Zarifi MK, Anthony DC, De Girolami U, Tarbell NJ, Black PM. Noninvasive magnetic resonance spectroscopic imaging biomarkers to predict the clinical grade of pediatric brain tumors. *Clin Cancer Res.* 2004; 10:8220–8228. [PubMed: 15623597]
  27. Tzika AA, Astrakas LG, Zarifi MK, Zurakowski D, Poussaint TY, Goumnerova L, Tarbell NJ, Black PM. Spectroscopic and perfusion magnetic resonance imaging predictors of progression in pediatric brain tumors. *Cancer.* 2004; 100:1246–1256. [PubMed: 15022293]
  28. Warren KE, Frank JA, Black JL, Hill RS, Duyn JH, Aikin AA, Lewis BK, Adamson PC, Balis FM. Proton magnetic resonance spectroscopic imaging in children with recurrent primary brain tumors. *J Clin Oncol.* 2000; 18:1020–1026. [PubMed: 10694552]
  29. Marcus KJ, Astrakas LG, Zurakowski D, Zarifi MK, Mintzopoulos D, Poussaint TY, Anthony DC, De Girolami U, Black PM, Tarbell NJ, Tzika AA. Predicting survival of children with CNS tumors using proton magnetic resonance spectroscopic imaging biomarkers. *Int J Oncol.* 2007; 30:651–657. [PubMed: 17273766]
  30. Thakur SB, Karimi S, Dunkel IJ, Koutcher JA, Huang W. Longitudinal MR spectroscopic imaging of pediatric diffuse pontine tumors to assess tumor aggression and progression. *AJNR Am J Neuroradiol.* 2006; 27:806–809. [PubMed: 16611768]
  31. Panigrahy A, Nelson MD Jr, Finlay JL, Spoto R, Krieger MD, Gilles FH, Bluml S. Metabolism of diffuse intrinsic brainstem gliomas in children. *Neuro Oncol.* 2008; 10:32–44. [PubMed: 18003889]

32. Laprie A, Pirzkall A, Haas-Kogan DA, Cha S, Banerjee A, Le TP, Lu Y, Nelson S, McKnight TR. Longitudinal multivoxel MR spectroscopy study of pediatric diffuse brainstem gliomas treated with radiotherapy. *Int J Radiat Oncol Biol Phys.* 2005; 62:20–31. [PubMed: 15850898]
33. Duyn JH, Gillen J, Sobering G, van Zijl PC, Moonen CT. Multisection proton MR spectroscopic imaging of the brain. *Radiology.* 1993; 188:277–282. [PubMed: 8511313]
34. Jacobs MA, Horska A, van Zijl PC, Barker PB. Quantitative proton MR spectroscopic imaging of normal human cerebellum and brain stem. *Magn Reson Med.* 2001; 46:699–705. [PubMed: 11590646]
35. Tedeschi G, Bertolino A, Campbell G, Barnett AS, Duyn JH, Jacob PK, Moonen CT, Alger JR, Di Chiro G. Reproducibility of proton MR spectroscopic imaging findings. *AJNR Am J Neuroradiol.* 1996; 17:1871–1879. [PubMed: 8933871]
36. Klein, JP.; Moeschberger, ML. Survival analysis techniques for censored and truncated data. New York, NY: Springer Science + Business Media Inc; 2003.
37. McKnight TR, Lamborn KR, Love TD, Berger MS, Chang S, Dillon WP, Bollen A, Nelson SJ. Correlation of magnetic resonance spectroscopic and growth characteristics within Grades II and III gliomas. *J Neurosurg.* 2007; 106:660–666. [PubMed: 17432719]
38. Law M, Yang S, Wang H, Babb JS, Johnson G, Cha S, Knopp EA, Zagzag D. Glioma grading: sensitivity, specificity, and predictive values of perfusion MR imaging and proton MR spectroscopic imaging compared with conventional MR imaging. *AJNR Am J Neuroradiol.* 2003; 24:1989–1998. [PubMed: 14625221]
39. Ng WH, Lim T. Targeting regions with highest lipid content on MR spectroscopy may improve diagnostic yield in stereotactic biopsy. *J Clin Neurosci.* 2008; 15:502–506. [PubMed: 18334298]
40. Balmaceda C, Critchell D, Mao X, Cheung K, Pannullo S, DeLaPaz RL, Shungu DC. Multisection 1H magnetic resonance spectroscopic imaging assessment of glioma response to chemotherapy. *J Neurooncol.* 2006; 76:185–191. [PubMed: 16151595]
41. Hayward RM, Patronas N, Baker EH, Vezina G, Albert PS, Warren KE. Inter-observer variability in the measurement of diffuse intrinsic pontine gliomas. *J Neurooncol.* 2008; 90:57–61. [PubMed: 18587536]
42. Yang I, Huh NG, Smith ZA, Han SJ, Parsa AT. Distinguishing Glioma Recurrence from Treatment Effect After Radiochemotherapy and Immunotherapy. *Neurosurgery Clinics of North America.* 2010; 21:181–186. [PubMed: 19944976]
43. Nelson MD Jr, Soni D, Baram TZ. Necrosis in pontine gliomas: radiation induced or natural history? *Radiology.* 1994; 191:279–282. [PubMed: 8134588]
44. Liu AK, Macy ME, Foreman NK. Bevacizumab as therapy for radiation necrosis in four children with pontine gliomas. *Int J Radiat Oncol Biol Phys.* 2009; 75:1148–1154. [PubMed: 19857784]
45. Castillo M, Kwock L. Proton MR spectroscopy of common brain tumors. *Neuroimaging Clin N Am.* 1998; 8:733–752. [PubMed: 9769340]
46. Tzika AA, Zarifi MK, Goumnerova L, Astrakas LG, Zurakowski D, Young-Poussaint T, Anthony DC, Scott RM, Black PM. Neuroimaging in pediatric brain tumors: Gd-DTPA-enhanced, hemodynamic, and diffusion MR imaging compared with MR spectroscopic imaging. *AJNR Am J Neuroradiol.* 2002; 23:322–333. [PubMed: 11847064]
47. Nelson SJ. Multivoxel magnetic resonance spectroscopy of brain tumors. *Mol Cancer Ther.* 2003; 2:497–507. [PubMed: 12748312]
48. Senft C, Hattingen E, Pilatus U, Franz K, Schanzer A, Lanfermann H, Seifert V, Gasser T. Diagnostic value of proton magnetic resonance spectroscopy in the noninvasive grading of solid gliomas: comparison of maximum and mean choline values. *Neurosurgery.* 2009; 65:908–913. discussion 913. [PubMed: 19834403]
49. Wagner M, Nafe R, Jurcoane A, Pilatus U, Franz K, Rieger J, Steinbach JP, Hattingen E. Heterogeneity in malignant gliomas: a magnetic resonance analysis of spatial distribution of metabolite changes and regional blood volume. *J Neurooncol.* 2010
50. Chen CY, Lirng JF, Chan WP, Fang CL. Proton magnetic resonance spectroscopy-guided biopsy for cerebral glial tumors. *J Formos Med Assoc.* 2004; 103:448–458. [PubMed: 15278190]

51. Lupo JM, Cha S, Chang SM, Nelson SJ. Analysis of metabolic indices in regions of abnormal perfusion in patients with high-grade glioma. *AJNR Am J Neuroradiol.* 2007; 28:1455–1461. [PubMed: 17846190]
52. Krieger MD, Bluml S, McComb JG. Magnetic resonance spectroscopy of atypical diffuse pontine masses. *Neurosurg Focus.* 2003; 15:E5. [PubMed: 15355007]
53. Barker PB, Lin DDM. In vivo proton MR spectroscopy of the human brain. *Progress in Nuclear Magnetic Resonance Spectroscopy.* 2006; 49:99–128.
54. de Graff, R. *In vivo* NMR spectroscopy: Principles and techniques. West Sussex, England: John Wiley & Sons; 2007.
55. Mascalchi M, Brugnoli R, Guerrini L, Belli G, Nistri M, Politi LS, Gavazzi C, Lolli F, Argenti G, Villari N. Single-voxel long TE 1H-MR spectroscopy of the normal brainstem and cerebellum. *J Magn Reson Imaging.* 2002; 16:532–537. [PubMed: 12412029]
56. McLean MA, Cross JJ. Magnetic resonance spectroscopy: principles and applications in neurosurgery. *Br J Neurosurg.* 2009; 23:5–13. [PubMed: 19234903]

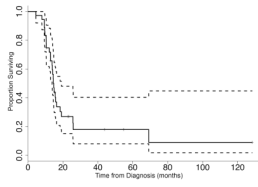


**Fig. 1.** Kaplan-Meier overall survival (OS) curve.  $n = 38$ ; median OS = 14.8 months (95% CI = 13.8, 19.1). Dotted lines represent 95% CI estimates.

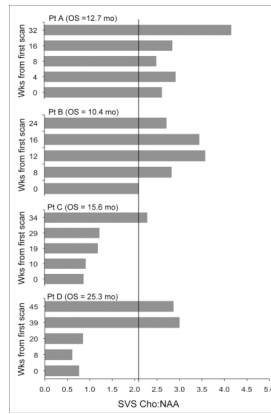


**Fig. 2.** Changes in SVS Cho:NAA for 4 patients on study (Solid black line indicates threshold at 2.1). Patients who had SVS Cho:NAA > 2.1 for all time points had a reduced survival compared to patients with lower SVS Cho:NAA values.



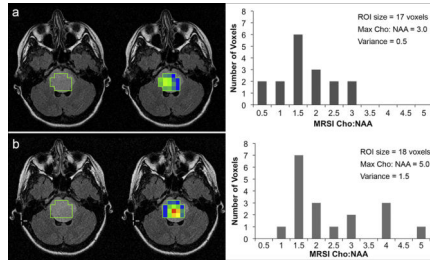


**Fig. 3.**

Changes in the variance of Cho:NAA values for one patient. FLAIR images with ROI selection (left), FLAIR images fused with Cho:NAA color maps (center) where blue = minimum, red = maximum (values range from 0.5 – 5.0) and histograms (right) showing the distribution of Cho:NAA values within each ROI. **a)** Results from the first scan on study. **b)** Results from the second scan on study (7 weeks later). The variance in Cho:NAA was much greater in the second scan. Overall survival for Patient was 13.6 months.

**Table 1**

## Clinical Data

	Patients		Median (Range)
	n	(%)	
Gender			
Male	13	(34%)	
Female	25	(66%)	
Age at Dx			5.3 yr (1.6 – 14.6 yr)
< 3 yr	4	(11%)	
3–5 yr	19	(50%)	
6–9 yr	8	(21%)	
10–12 yr	3	(8%)	
13–15 yr	4	(11%)	
Histological Grade at Dx			
Grade II astrocytoma	2	(5%)	
No Biopsy	36	(95%)	
Radiation Therapy			
RT alone	30	(79%)	
RT+	6	(16%)	
Dx to RT	36	(95%)	14 days (6 – 1559 days)
RT Dose	36	(95%)	54.0 Gy (50.4 – 61.2 Gy)

Dx = diagnosis, RT= radiation therapy, RT+ = RT and concurrent chemotherapy

**Table 2**

Univariate analyses of MRS measurements on overall survival

Variable	Hazard Ratio <sup>I</sup>	
	First MRS	Follow-up MRS
SVS		
Cho:NAA	1.38*	1.50 <sup>†</sup>
Cho:Cr	1.33	1.23
+Lac/Lip	1.95	1.67
MRSI		
Max Cho:NAA	1.06	1.39
Max Cho:Cr	1.29	1.15
Cho:NAA Variance	1.03	2.61*
Cho:Cr Variance	1.01	1.79

<sup>I</sup> Expresses the risk of mortality for a 1.0 change in the variable

\* p<0.05

<sup>†</sup> p<0.01

**Table 3**

Mortality risk associated with changes at follow-up

Change in Variable	Hazard Ratio	
	SVS Cho:NAA (p=0.009)	MRSI Cho:NAA Variance (p=0.03)
-1.00	0.67	0.38
-0.75	0.74	0.49
-0.50	0.82	0.62
-0.25	0.90	0.79
+0.25	1.11	1.27
+0.50	1.22	1.61
+0.75	1.35	2.05
+1.00	1.50	2.61